Nanoscale

PAPER

View Article Online
View Journal | View Issue

Cite this: *Nanoscale*, 2025, **17**, 16672

Ultrasound activated silica particles for efficient eradication of dental biofilms†

Menisha Manhota,‡[a,b] Maria L. Odyniec,‡[a] Grace Ball,[a] Daniel J. Bell,[a] Rininta Firdaus,[a] Feng Wang,[c] Yu-Lung Chiu,[c] Rachel L. Sammons,[d] Sarah A. Kuehne,*[d,e] A. Damien Walmsley*[b,d] and Zoe Pikramenou*[a,b]

Dental infections and diseases are a global health problem, affecting more than 3.5 billion people worldwide. Bacterial biofilms are dominant contributors to oral disease and their treatment is challenging due to increased antimicrobial resistance and reduced efficiency of drug penetration. Low frequency ultrasound is an attractive stimulus for drug delivery systems with controlled, low power that does not interfere with chemical reactivity but may only influence intermolecular chemical interactions in localised applications. We present an ultrasound triggered nanodelivery system for localised treatment of biofilms. Our nanodelivery system is based on an antibacterial agent, cetylpyridinium chloride (CPC), incorporated as micelles within the silica particle framework (**m-CPC⊂SiO$_2$**) which is only released by application of low frequency ultrasound, circumventing uncontrolled, "burst", drug leakage. Ultrasonic exposure of **m-CPC⊂SiO$_2$** from a clinical dental ultrasonic scaler device leads to release of CPC, not observed in the absence of ultrasound. High resolution electron microscopy of **m-CPC⊂SiO$_2$** on exposure to ultrasound reveals changes in the structural framework of the particles and reveals voids confirming release of CPC. The antimicrobial efficacy of the **m-CPC⊂SiO$_2$** nanosystem is investigated against 72 h single species *Streptococcus sanguinis* biofilms, a common dental bacterium. The ultrasound-activated **m-CPC⊂SiO$_2$** nanosystem shows improved antimicrobial activity leading to a 10 000-fold reduction in colony forming units of bacteria compared to treatment with only CPC. This approach is a transformative strategy for controlled and localised delivery of antibiotics for dental and medical applicatons in different clinical settings.

Received 14th March 2025,
Accepted 18th June 2025

DOI: 10.1039/d5nr01091h

rsc.li/nanoscale

Introduction

Oral diseases such as dental caries and periodontal disease are largely preventable but present a high burden for the population. Dental caries is a biofilm-mediated, sugar-driven, dynamic disease which results in the destruction of enamel and dentine in teeth.[1] Severe periodontal disease affects around 10% of the world's population with an associated cost of ~£500 billion.[2,3] There is an emerging need for new therapies to reduce this burden of disease. Biofilm mediated infections create challenges in the delivery and maintenance of sufficient drug concentrations at the site of infection.[4,5] Bacteria in biofilm develop different physiological states, slow growth and are up to 1000 times more resistant to antibiotics compared to planktonic organisms.[6,7]

Due to the widespread use of dental scalers in oral healthcare, we sought to develop an ultrasound triggered drug delivery system based on nanoparticles for effective treatment of biofilm-based oral infections. A dental scaler is a handheld device capable of generating ultrasonic vibrations used to 'deep clean' teeth. The ultrasonic vibration from the dental scaler disrupts and dislodges plaque (dental biofilms) and mineralised biofilms termed calculus (calcified plaque).[8–10] In the removal of biofilms, the ultrasonic scaler produces cavitation. Cavitation is the rapid rise and collapse of gas bubbles produced due to a drop in the negative pressure caused by low frequency ultrasound in solution.[11,12] Although cavitation effects have been shown in clinical studies to be efficient for biofilm removal, this remains challenging at the subgingival level, below the gumline, due to limited access and visibility.[13,14] It is increasingly difficult to eradicate bacteria especially if they have

[a]*School of Chemistry, College of Engineering and Physical Sciences, University of Birmingham, Edgbaston, Birmingham, B15 2TT, UK.*
E-mail: z.pikramenou@bham.ac.uk
[b]*Physical Sciences for Health Centre, University of Birmingham, Edgbaston, Birmingham B15 2TT, UK*
[c]*School of Metallurgy and Materials, College of Engineering and Physical Sciences, University of Birmingham, Edgbaston, Birmingham, B15 2TT, UK*
[d]*School of Dentistry, College of Medical and Dental Sciences, University of Birmingham, Birmingham, B5 7EG, UK*
[e]*School of Science and Technology, Nottingham Trent University, Nottingham, UK*
†Electronic supplementary information (ESI) available. See DOI: https://doi.org/10.1039/d5nr01091h
‡Authors contributed equally.

reached and entered the dentinal tubules which become exposed in periodontally diseased teeth.[15–17]

In the field of drug delivery systems, SiO_2 nanoparticles are attractive for their biocompatibility and tuneable sizing. Mesoporous SiO_2 particles have a periodic porous structures to incorporate various drug molecules and have dominated the drug delivery approaches due to the high surface area of the porous structure that allows drug adsorption.[18] However, release from traditional mesoporous frameworks is governed by diffusion, leading to uncontrolled and "burst", off-target drug leakage from their pores. Additionally, the traditional preparation of a porous silica framework requires the use of a surfactant template *i.e.* cetyltrimethylammonium bromide which is subsequently removed. To avoid the use of these toxic agents, micelles of amphiphilic antimicrobial compounds as a non-cytotoxic removable template in the sol–gel synthesis of silica nanocontainers have been proposed.[19–22] An alternative approach to controlling off-target drug leakage is functionalising the silica surface with coatings or internal modifications to reversibly block the pores.[18,23] Such controlled drug release systems have been developed that are responsive to stimuli such as enzymes,[24,25] pH,[26,27] redox conditions,[28,29] light,[30] temperature[31] and magnetic fields.[32,33] High frequency ultrasound (>1 MHz) as a trigger has been used in covalent bond breaking to release polymers or supramolecules from silica surface[23,34–38] In our approach we aim to use low-frequency ultrasound to control release of agents from the silica framework. We have previously introduced modification of SiO_2 for detection and drug delivery[39–42] as well as penetration of SiO_2 within dental tubules in molar root tooth sections by electron and optical microscopies.[43,44] The acoustic cavitation behaviour produced from an ultrasonic dental scaler proved to enhance the SiO_2 particle penetration increasing from 60 μm to ~180 μm on application of ultrasound within the dentinal tubules.[44] A stimuli-controlled delivery system that can deliver an antimicrobial into these difficult to reach tubules and eradicate biofilms would therefore have great clinical utility.

Herein, we demonstrate that encapsulated micelles of cetylpyridinium chloride (m-CPC) within the SiO_2 particle framework, **m-CPC⊂SiO$_2$**, release the antimicrobial agent CPC only upon application of low frequency ultrasound (Fig. 1). CPC is an antibacterial amphiphile with a positively charged quaternary ammonium headgroup and a hexadecyl aliphatic tail, widely used in dental products such a mouthwashes.[45] CPC has broad spectrum antimicrobial properties *via* interaction with lipids and proteins of the bacterial cell membrane, which leads to disorganisation in its structure and leakage of low-molecular weight components out of the cell.[45] CPC forms micelles in solution and has a critical micelle concentration of 1×10^{-3} M in pH neutral aqueous solutions at 25 °C.[46] We have previously demonstrated that CPC can form micelles with other antibiotics incorporated into the micelle structure, coupled with encapsulation into SiO_2.[42] Our studies showed that dual antimicrobial delivery can be achieved through this method. In this study, we aim to further investigate the use of **m-CPC⊂SiO$_2$** for ultrasound activated release and biofilm eradication. We investigate the activity of **m-CPC⊂SiO$_2$** *in vitro* and against single species biofilms of the model organism *Streptococcus sanguinis* (*S. sanguinis*), to demonstrate controlled, localised, triggered delivery of CPC. *S. sanguinis* was selected as a biofilm model due to its predominance in the human oral cavity and its high abundance in dental biofilm communities.[47,48] *S. sanguinis* is equally present in healthy and diseased states,[48] and serves as a pioneer colonizer in biofilm formation. *S. sanguinis* is often found at the base of polymicrobial biofilm communities implicated in gingivitis, periodontitis, peri-implantitis, dental caries and root canal infections.[47] Furthermore, dental plaque containing *S. sanguinis* is a concomitant risk factor in development of acute coronary syndrome.[49] Importantly, *S. sanguinis* plays a regulatory role in shaping the oral microbiome through interspecies interactions. It produces hydrogen peroxide *via* pyruvate oxidase (SpxB), which inhibits the growth of cariogenic species such as *Streptococcus mutans*, thereby contributing to microbial homeostasis and preventing dysbiosis.[50,51] This ecological function makes *S. sanguinis* a valuable model for studying early-stage biofilm dynamics and for evaluating strategies aimed at disrupting biofilm maturation before pathogenic

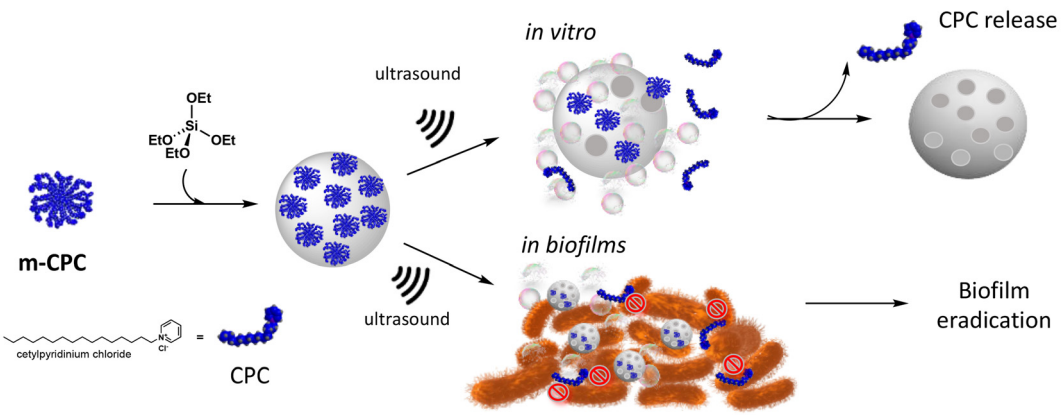

Fig. 1 Ultrasound triggered release strategy from **m-CPC⊂SiO$_2$**.

species become established. By targeting early colonizers such as *S. sanguinis*, our approach offers a preventive strategy for biofilm-associated diseases. Furthermore, the platform described in this study can be readily adapted to target recognised oral pathogens in future investigations, thereby broadening its clinical relevance and therapeutic potential. We employ high resolution electron microscopy is employed to study the effect of ultrasound on the silica framework of **m-CPC⊂SiO$_2$** upon drug release and confocal imaging microscopy to demonstrate the local effect in biofilm eradication.

Results and discussion

Characterisation of silica nanoparticles

m-CPC⊂SiO$_2$ were synthesised by addition of a solution containing CPC above the critical micelle concentration into a silica pre-formed core (3 h silica growth), followed by subsequent completion of silica growth for 6 h. The same methodology was followed for synthesis of unloaded SiO_2 without CPC (ESI Fig. S1, Table S1†). The average sizes **m-CPC⊂SiO$_2$** particles were examined by dynamic light scattering (DLS) and Scanning Electron Microscopy (SEM). DLS data shows average diameter measured by intensity as 420 ± 50 nm (PDI = 0.23) and image analysis of sizes by SEM gives an average diameter of 340 ± 60 nm (PDI = 0.03, n = 50) (Fig. 2). The larger size by DLS is attributed to differences in measurement techniques as DLS considers the hydrodynamic radius of particles in solution whereas SEM measures a dried sample. Moreover, the surface charge measured by ζ-potential gives a value of −32 ± 6 mV (Table S1†). The negative ζ-potential indicates that the positively charged CPC is not associated with the surface of the nanoparticle. The inclusion of m-CPC into the silica framework was investigated using MALDI-ToF mass spectrometry and solid-state UV-Vis absorption (Fig. 2). MALDI-ToF analysis of **m-CPC⊂SiO$_2$** shows a peak at m/z 304 attributed to the cetylpyridinium ion and loss of chloride salt ($[C_{21}H_{38}N]^+$), confirming the presence of CPC in **m-CPC⊂SiO$_2$**. In addition, the solid-state absorption spectrum of **m-CPC⊂SiO$_2$** shows a band at 260 nm, corresponding to CPC (Fig. 2). Finally, quantitative measurements of drug loading were carried out by UV-Vis spectroscopy of the reaction supernatant and thermogravimetric analysis (TGA). The encapsulation efficiency of CPC in **m-CPC⊂SiO$_2$** based on UV-Vis spectroscopy studies of the synthesis supernatant was calculated as 8.3% (equation ESI†) based on the difference between the initial concentration of CPC in the reaction mixture and CPC remaining in the supernatant. TGA continuously monitors sample weight loss upon heating at a defined rate under a controlled atmosphere. The amount of organic composition (μg mg^{-1}) was calculated from the TGA weight loss from 150 to 800 °C. Compared to unloaded SiO_2, **m-CPC⊂SiO$_2$** showed a weight loss of 7.7% corresponding to encapsulation of CPC, with drug loading of 77 μg_{CPC} per mg_{SiO_2} (Fig. 2). Control particles were also synthesised to compare the release profiles from surface association based on an MCM-41 framework. MCM-41 particles were synthesised with CPC micelle instead of cetyltrimethylammonium bromide in order to compare the release from micelles inside the silica network according to the conditions of forming mesopores and are noted, as **CPC⊂MCM-41**. MCM-41 particles, traditionally synthesised and calcinated, with CPC adsorbed in the mesopores are noted as

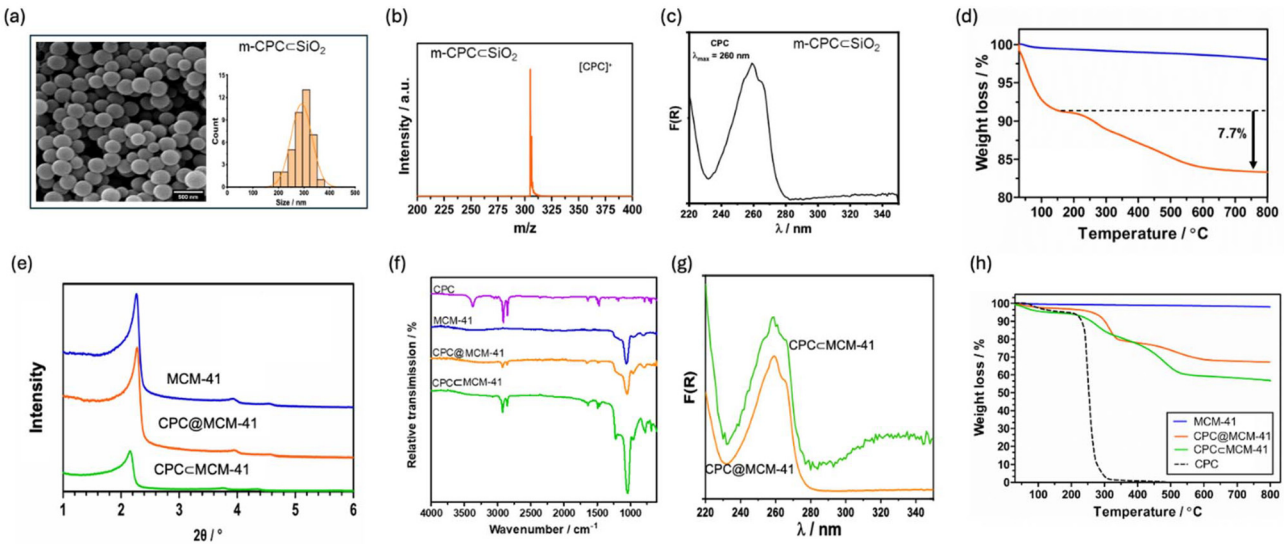

Fig. 2 Top: Characterisation of **m-CPC⊂SiO$_2$**. (a) Scanning electron microscopy accompanied by a histogram of the size measurements (n = 40); (b) MALDI-TOF MS showing CPC presence; (c) solid state UV-Vis spectroscopy showing a characteristic peak for CPC, where $F(R) = (1 - R)^2/2R$, R = reflectance, (d) TGA comparison of **SiO$_2$** and **m-CPC⊂SiO$_2$**, measured from 100 °C to account for loss of water (sample = 10 mg). Bottom: Characterisation of MCM-41 particles with CPC; (e) SAXS patterns of **MCM-41**, **CPC@MCM-41** and **CPC⊂MCM-41**. (f) FTIR spectra of CPC, **MCM-41**, **CPC@MCM-41** and **CPC⊂MCM-41**; (g) solid-state UV-Vis spectroscopy of particles where $F(R) = (1 - R)^2/2R$, R– reflectance and (h) TGA curves showing the weight loss profiles with heating rate of 10 °C min^{-1} from 30 to 800 °C under nitrogen atmosphere.

CPC@MCM-41 and were used to compare surface induced CPC release.[52] DLS data show average diameter measured by intensity as 135 ± 25 nm (PDI = 0.37) and 200 ± 53 nm (PDI = 0.31) for **CPC@MCM-41** and **CPC⊂MCM-41** respectively (Table S2†). The surface charge measured by ζ-potential gives values of +4 ± 5 mV and +36 ± 5 mV for **CPC@MCM-41** and **CPC⊂MCM-41** respectively, indicating the presence of positively charged CPC near the SiO_2 surface, which is more prominent in **CPC⊂MCM-41** possibly due to orientation of CPC during templating step as opposed to adsorption of CPC in **CPC@MCM-41** (Table S2†). They were further characterised by small angle powder X-ray diffraction (SAXS), infrared spectroscopy (FTIR) and solid state UV-Vis spectroscopy to demonstrate the presence of CPC (Fig. 2). Diffraction patterns by SAXS for **CPC@MCM-41** and **CPC⊂MCM-41** show patterns with 2θ = 2.2° and two smaller peaks at 3.9° and 4.5° indexed to (100), (110) and (200) respectively, at 3.9° and 4.5° indexed to (100), (110) and (200) respectively, characteristic of 2D hexagonal mesoporous structure of MCM-41 nanoparticles. The peaks for **CPC⊂MCM-41** are shifted to lower 2θ angles, showing a small increase in pore size.[52] FTIR and UV-Vis spectroscopy confirm the presence of CPC. TGA weight loss from 150 to 800 °C shows a weight loss of 47% and 44% corresponding to CPC for **CPC@MCM-41** and **CPC⊂MCM-41** respectively. Their profiles of the *in vitro* release studies are compared in the following section with the particles without mesoporous structures.

In vitro drug release of m-CPC⊂SiO_2

The drug release behaviour in static conditions and post-ultrasound irrigation was investigated for **m-CPC⊂SiO_2** particles *in vitro* by immersing an ultrasonic scaler in the nanoparticle suspension. The CPC drug release was monitored by UV-Vis spectroscopy based on the absorbance of CPC (λ_{max} = 260 nm, ε = 4190 M^{-1} cm^{-1}). The particle suspension was exposed to 2 min pulses of ultrasound at the maximum power setting, P20 (100 mA, 1 W) and cumulative release calculated. CPC release is significantly enhanced by ultrasound, after a total of 10 min ultrasound, CPC release reached 9.8 ± 3.3 μg_{CPC} per mg_{SiO_2}, equating to a 13% release efficiency (Fig. 3). Under static conditions, less than 1% of CPC was released from **m-CPC⊂SiO_2**. At power settings P10 (52 mA, 0.27 W) and P15 (76 mA, 0.58 W), CPC release reached 6.5 ± 0.3 μg_{CPC}per mg_{SiO_2} and 7.8 ± 0.4 μg_{CPC} per mg_{SiO_2} respectively (Fig. 3, Fig. S2†). Application of ultrasound exposes drug delivery systems to mechanical, thermal and chemical effects.[53] Transient cavitation has been shown to occur at dental scaler tip, with an increased number of cavitation bubbles growing and collapsing at higher power settings.[54] Collapse of cavitation bubbles is violent and can result in the generation of high velocities, pressures, and temperatures.[55] We attribute the increase in release at higher power settings to a combination of mechanical and chemical effects. At 37 °C, our measured thermal increase due to application of ultrasound is 2.1 ± 1.3 °C and 3.6 ± 2.1 °C at P10 (0.27 W) and P20 (1 W) respectively. The difference in temperature is likely to have a negligible contribution to drug release at different power settings.[56] The chemical effects of cavitation are measured using potassium iodide dosimetry where the rate of formation of triiodide ion formation is used as a quantitative measure of acoustic cavitation as hydroxyl radicals generated by pyrolysis of water oxidise potassium iodide.[57,58] Measurements of I_3^- formation show the reaction rate of oxidation increases with increasing electrical power up to P15 (0.58 W) (Fig. S3†). The additional drug release observed from P15 (0.58 W) to P20 (1 W) is attributed to an increase in mechanical effects at higher power settings. Experimental studies have previously correlated increased drug release with higher power and an increase in ultrasound-induced cavitation from soft materials.[59–61] The mechanical stress generated by application of ultrasound is reported to be responsible for the breakage of covalent bonds, non-covalent π–π interactions, metal coordination and hydrogen bonds.[62] Ultrasound can induce flexibility to the silica chains and in some cases causes damage to the drug delivery system breaking it apart, resulting in accelerated expulsion of drugs.[23] In contrast, CPC release profiles of **CPC@MCM-41** and **CPC⊂MCM-41** show different release profiles. Under static conditions, **CPC@MCM-41** shows a burst release with 0.8 ± 1.1 μg_{CPC} per mg_{SiO_2} after 2 min which is unchanged after 10 min. An increased release is observed on application of ultrasound (P20, 1 W, 2 min exposure, 10 min total) to 8.3 ± 0.4 μg_{CPC} per mg_{SiO_2}, with no change of the release profile

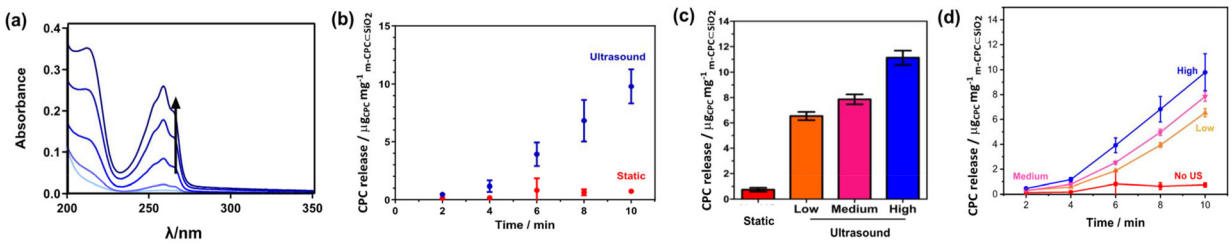

Fig. 3 Drug release profiles of **m-CPC⊂SiO_2** (2 mg mL^{-1}, H_2O, 37 °C, pH 7.4) before and after ultrasonication. **m-CPC⊂SiO_2** particles were exposed to ultrasound (2 min pulses for a total of 10 min). The release was monitored by CPC absorbance band at λ_{max} = 260 nm. (a) Selected UV-Vis spectra after exposure to ultrasound (P20); (b) quantification of CPC release per mg of **m-CPC⊂SiO_2** after each exposure to static or ultrasound (P20) conditions; (c) overall amount of CPC released from **m-CPC⊂SiO_2** at different ultrasound power settings (low-P10, medium-P15, high-P20) after 10 min irrigation and (d) at different time intervals. Mean values with standard deviation are plotted.

(Fig. S4†). Additionally, **CPC⊂MCM-41** shows an uncontrolled sustained release profile in static conditions, reaching 10.5 ± 0.5 μg_{CPC} per mg_{SiO_2}, increasing to 29.9 ± 1.5 μg_{CPC} per mg_{SiO_2} after application of ultrasound (P20, 1 W, 2 min exposure, 10 min total). The difference in release in static and ultrasound conditions is attributed to mechanical stress from ultrasound breaking more supramolecular interactions between positively charged CPC and negatively charged silica framework.[62] These release profiles highlight the advantages of using **m-CPC⊂SiO$_2$** as a drug delivery systems as it has remarkable static stability and controlled ultrasound triggered release of CPC.

The morphological changes of **m-CPC⊂SiO$_2$** particles exposed to static and ultrasound conditions were investigated using electron microscopy techniques. Scanning Electron Microscopy (SEM) reveals the uniform and spherical nature of **m-CPC⊂SiO$_2$** particles were maintained after ultrasound stimulation in water and measured sizes remaining the same; 340 ± 60 nm (PDI = 0.03, n = 50) and 325 ± 50 nm (PDI = 0.03, n = 50) pre- and post-ultrasound, respectively (Fig. S5†). Scanning transmission electron microscopy (STEM) techniques were employed to investigate changes on the particle surface pre- and post-ultrasound irrigation. The brightfield TEM micrographs showed a smooth texture of the **m-CPC⊂SiO$_2$** particles attributing to a solid and high mass density with no apparent porous network before exposure to ultrasound (Fig. 4). This is in contrast with the unidimensional porous network for **CPC@MCM-41** and **CPC⊂MCM-41** (Fig. S6†). Following exposure to ultrasound irrigation in aqueous solution (P20, 1 W, 10 min), brightfield TEM revealed alterations to the surface of **m-CPC⊂SiO$_2$**. Roughness of the exterior silica shell is clearly seen (Fig. 5) with slight deformations of the smooth surface of **m-CPC⊂SiO$_2$**. Remarkably with High-Angle Annular Dark-Field Scanning Transmission Electron Microscopy (HAADF-STEM), dark and small circular features were apparent, with estimated diameter size of 4.7 ± 1.1 nm (n = 50). These features match the CPC micelle size and are attributed to the release of m-CPC and a remaining non-periodic porous structure. These studies demonstrate the importance of STEM techniques in monitoring structural and morphological effects upon low frequency ultrasound and concomitant drug release from the SiO_2 framework. To further elucidate the structural changes of **m-CPC⊂SiO$_2$**, we chose to study the release of CPC in dispersions of **m-CPC⊂SiO$_2$** particles in methanol which is known to disrupt micelles through chemical trapping.[63] SEM analysis shows a crinkle-like texture on the surface of **m-CPC⊂SiO$_2$**, although the overall size (355 ± 56 nm, PDI = 0.02) and shape of nanoparticles was unaltered (Fig. S7†). HAADF-STEM shows prominent dark circular features with an estimated size of 6.5 ± 1.6 nm (n = 50). The same features are also observed in the brightfield TEM image as bright circular topographies with darker ring outlines (Fig. 4). These results reinforce the structural changes caused by CPC release from **m-CPC⊂SiO$_2$** as observed in aqueous solutions and methanol.

Energy Dispersed X-ray Spectroscopy (EDS) mapping was further used to characterise the elemental composition of the particles. The predominant presence of silicon and oxygen, from the nanoparticle framework and nitrogen arising from the encapsulated CPC is clearly observed (Fig. 5) for **m-CPC⊂SiO$_2$** particles with and without ultrasound (P20, 10 min) and in MeOH. The mapping of silicon, oxygen and nitrogen in **m-CPC⊂SiO$_2$** shows there is no difference in distribution of silicon and oxygen in the nanoparticle framework and nitrogen from the encapsulated CPC, indicating a uniform distri-

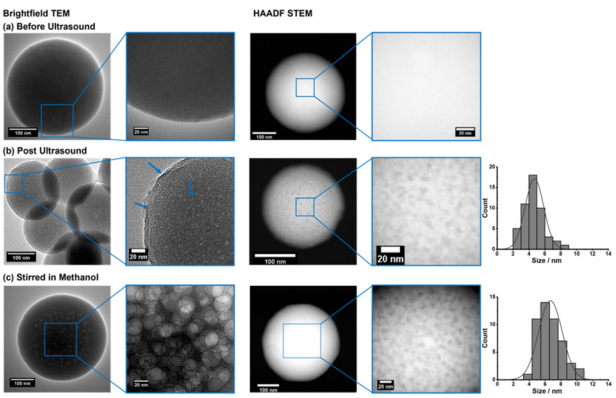

Fig. 4 Brightfield and high-angle annular dark-field-scanning transmission electron microscopy (HAADF-STEM) images of of **m-CPC⊂SiO$_2$** (a) before ultrasound in water; (b) post-ultrasound (P20, 10 min) in water and (c) in methanol showing features which match m-CPC size. Brightfield magnification 49–295 kX, 300 kV electron beam; HAADF-STEM magnification from 190 to 540 kX. 300 kV electron beam. Histogram of sizes plotted for voids observed in HAADF-STEM are based on 50 independent measurements.

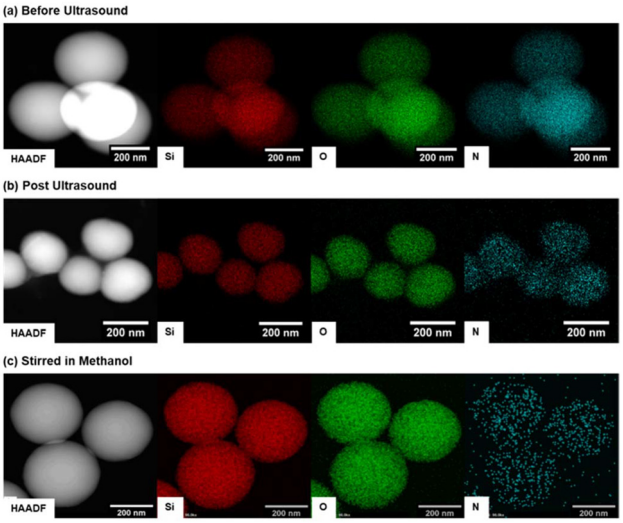

Fig. 5 High-angle annular dark-field-scanning transmission electron microscopy (HAADF-STEM) and energy dispersive X-ray mapping (EDS) to show distribution of silicon (Si), oxygen (O) and nitrogen (N) of **m-CPC⊂SiO$_2$** (a) pre-ultrasound in water, (b) post ultrasound (P20, 10 min) in water and (c) after stirring in methanol (72 h). HAADF-STEM magnification from 190–540 kX, 300 kV electron beam.

bution of CPC within the nanoparticle. After exposure to ultrasound irrigation in water, there is a change in nitrogen distribution in **m-CPC⊂SiO$_2$** compared to silicon and oxygen and qualitative reduction in observed nitrogen signal, which supports loss of nitrogen and therefore release of CPC. Upon stirring in methanol, there is a distinct difference and reduction of the nitrogen signal from remaining CPC and silicon and oxygen signal from the nanoparticle framework, further supporting that CPC is released from **m-CPC⊂SiO$_2$** upon ultrasound irrigation and stirring in methanol.

To investigate the particle porosity induced by CPC release, nitrogen porosimetry isotherms were examined before and after exposure to ultrasound in water and methanol (Fig. 6). The nitrogen porosimetry isotherms of **m-CPC⊂SiO$_2$** untreated and after exposure to ultrasound (P20, 1 W, 10 min) exhibit a Type I(a) isotherm, according to IUPAC classification, characteristic of microporous materials with relatively low surface area. The synthesised particles have a Brunauer, Emmett and Teller (BET) surface area of 16.5 ± 0.2 m^2 g^{-1} which has an increase to 25.4 ± 0.3 m^2 g^{-1} after exposure to ultrasound irrigation (10 min total, P20, 1 W) in H_2O. The increase in BET surface area is attributed to the 16% release efficiency upon exposure to ultrasound and an increase in porosity on release of CPC as observed in HAADF-STEM (Fig. 5). After stirring in MeOH the nanoparticles have an estimated BET surface area of 87.8 ± 1.5 m^2 g^{-1}, a pore size of 2.5 nm (Fig. 6) and display a Type II isotherm characteristic of microporous materials with narrow pore size. A type IV isotherm and type H1 hysteresis loop are not observed, suggesting the absence of unidimensional pores observed with MCM-41 particles, these data support the non-periodic pore structure observed in HAADF-STEM (Fig. 4).

Ultrasound-triggered release of CPC from m-CPC⊂SiO$_2$ in single-species biofilm models

To study the ultrasound responsive nature of **m-CPC⊂SiO$_2$** for delivery of CPC, single species *S. sanguinis* planktonic cultures and 72 h biofilm models were used. Initially, the Minimum Inhibitory Concentration (MIC) of unloaded SiO_2 and CPC against planktonic cultures of *S. sanguinis* was assessed. The MIC of CPC was <6 μg mL^{-1} and unloaded SiO_2 displayed no antimicrobial activity, even when tested at concentrations as high as 16 mg mL^{-1} (Fig. S8†). The antimicrobial activity was further analysed by zones of inhibition formed during an agar diffusion assay with silica-drug formulations without ultrasound. Table 1 displays the zone diameters of CPC, SiO_2, and **m-CPC⊂SiO$_2$** against *S. sanguinis* and compared to a control silica-drug formulation where CPC had been adsorbed onto the surface of mesoporous silica nanoparticles, **CPC@MCM-41** (2 mg mL^{-1}) or templated within mesoporous silica nanoparticles, **CPC⊂MCM-41** (2 mg mL^{-1}). The zone sizes from CPC (0.05% w/v), **CPC⊂MCM-41** (2 mg mL^{-1}) and **CPC@MCM-41** (2 mg mL^{-1}) were estimated to be 13 ± 1 mm, 12 ± 2 mm and 16 ± 2 mm, respectively. **SiO$_2$** (10 mg mL^{-1}) and **m-CPC⊂SiO$_2$** (10 mg mL^{-1}) showed no inhibition after 24 h (Fig. S9†). A concentration of CPC at 0.05% w/v was chosen as it is the concentration commonly found in mouthrinses.[64] These data show that application of CPC uncontrollably kills bacteria and templated **CPC⊂MCM-41** and adsorbed **CPC@MCM-41** experience rapid leakage of CPC. In comparison, encapsulation of CPC in **SiO$_2$** as synthesised in this work, protects CPC from being released in the bacterial environment without a trigger.

The delivery of **m-CPC⊂SiO$_2$** for triggered release and delivery of antimicrobials to biofilms was investigated using a 72 h *S. sanguinis* biofilm. Firstly, SEM analysis was used to examine the appearance of the biofilms and changes with the application of treatment and/or ultrasound (P10, 0.27 W, 10 s). Fig. 7 shows that *S. sanguinis* typically displayed chains or pairs of oval shaped cocci and upon cavitation exposure the overall architecture of the biofilm changed. The long chains of cocci appeared to have separated and a string-like network was observed. This indicates that the ultrasonic device had mechanically disrupted the biofilm matrix due to the acoustic cavitation produced from the ultrasound,[65,66] exposing and disrupting the EPS matrix, appearing as thread like strands. The morphology of the bacterial cells had not changed and they appeared to be structurally undamaged. The same changes occurred when treated with CPC (0.05% w/v) and ultrasound (P10, 0.27 W, 10 s). On application of **m-CPC⊂SiO$_2$** particles (10 mg mL^{-1}) and ultrasound (P10, 0.27 W, 10 s), the SEM images show EPS threads, attributed to the application of ultrasound and spheres smaller in size than *S. sanguinis* bac-

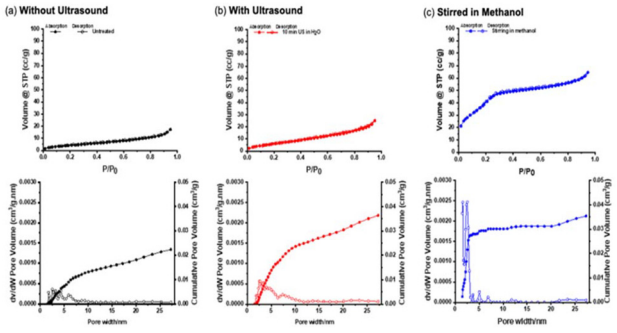

Fig. 6 Nitrogen adsorption–desorption isotherms at 77 K and calculated pore size distribution of **m-CPC⊂SiO$_2$** (a) untreated (b) after treatment with US (10 min, P10) and (c) after stirring in methanol for 72 h.

Table 1 Antibacterial activity displayed by zones of growth inhibition around wells with 50 μL using an agar diffusion assay. The diameters of the zones of inhibition were measured and averages calculated (n = 3). Plates inoculated with *S. sanguinis*

Sample	Concentration	Zone of inhibition
CPC	0.05% (w/v)	13 ± 1 mm
SiO_2	10 mg mL^{-1}	No inhibition
H_2O	50 μL	No inhibition
m-CPC⊂SiO$_2$	2 mg mL^{-1}	No inhibition
m-CPC⊂SiO$_2$	10 mg mL^{-1}	No inhibition
CPC@MCM-41	2 mg mL^{-1}	12 ± 2 mm
CPC⊂MCM-41	2 mg mL^{-1}	16 ± 2 mm

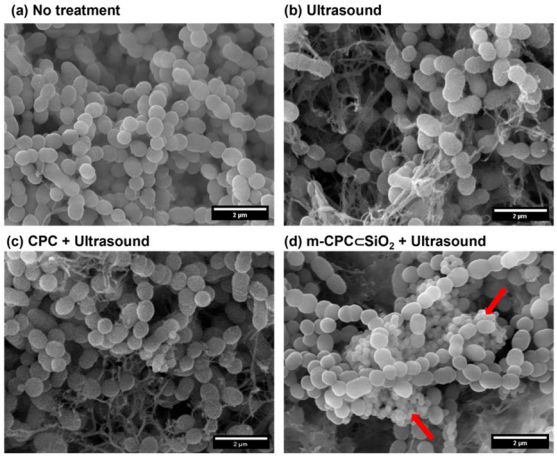

Fig. 7 SEM images of *S. sanguinis* biofilms showing effect of ultrasound and presence of particles. (a) no treatment; (b) treated with (ultrasound only P10 10 s); (c) CPC (14 μg mL^{-1}) + ultrasound (P10, 0.27 W, 10 s) and (d) **m-CPC⊂SiO$_2$** (10 mg mL^{-1}) + ultrasound (P10, 10 s). Red arrows indicate the presence of **m-CPC⊂SiO$_2$**. SEM magnification 10–20 kX, 20.0 kV electron beam. Scale bar represents 2 μm in each image.

teria (Fig. 7). The spheres are the same size as **m-CPC⊂SiO$_2$** particles, indicating the particles are present and can penetrate between the bacterium within the biofilm. SEM analysis confirms the disruption of the *S. sanguinis* biofilm by ultrasound and confirms the presence of particles within the biofilm on application of ultrasound.

The effect of ultrasound and particles on biofilms was also investigated using LIVE/DEAD staining for bacterial viability and confocal laser scanning microscopy alongside Colony Forming Unit (CFU) counting.[67] Initially, the effect of ultrasound on biofilms was investigated. At the maximum power setting (P20, 1 W), the application of ultrasound for 2 min removed most of the biofilm from coverslips, such that confocal fluorescence imaging could not be performed.[66,68] Furthermore, in a dental clinic setting, 2 min ultrasound is too long for continuous patient treatment at the highest power setting and may cause damage to the tooth. Previously, significant removal of bacteria from dental implant surfaces using the same dental ultrasonic scaler has been shown at power setting P10 (0.27 W) for 60 s at a distance of 1 mm from the surface.[69] In subsequent experiments the ultrasonic scaler was positioned at a fixed height of 10 mm with the tip parallel to the biofilm and individual biofilms were exposed to power setting P10 (0.27 W) for 5 or 10 s. *Z*-stack 3D reconstruction shows *S. sanguinis* viability remained consistent throughout the biofilm (up to 22 μm, >90% viability) and exposure to ultrasound did not cause complete removal of the biofilms (Fig. S10†). Therefore, parameters established for treatment of biofilms using ultrasonic scaler were 10 s at power setting P10 (0.27 W), 10 mm from biofilm surface. The time taken for antimicrobial effect of **m-CPC⊂SiO$_2$** after exposure to ultrasound on *S. sanguinis* biofilms was explored. After treatment, biofilms were incubated at 37 °C for 5, 15 and 30 min and bacterial viability was assessed to examine if incubation time increased killing. Analysis of *z*-stack images of biofilms treated with **m-CPC⊂SiO$_2$** and cavitation show an average cell viability of 52 ± 23%, 48 ± 25% and 4 ± 3%, respectively (Fig. S11 and S12†). Statistical analysis revealed incubation time after cavitation had a significant impact on bacterial viability ($P < 0.0001$ *vs.* untreated biofilm). This study illustrates that the longer the incubation time the increase in killing action of the biofilm, establishing a 30 min incubation period of *S. sanguinis* biofilms after treatment.

Following the optimisation of conditions, the effect of different treatments on *S. sanguinis* biofilms were investigated by confocal microscopy of LIVE/DEAD stained biofilms (Fig. 8). The *S. sanguinis* biofilms were treated with exposure to CPC (13 μg mL^{-1}), **SiO$_2$** (10 mg mL^{-1}) and **m-CPC⊂SiO$_2$** (10 mg mL^{-1}) before and post ultrasound (P10, 0.27 W, 10 s). Plate counts (CFU per mL) were conducted in parallel to verify viability and ultimately determine the efficacy of **m-CPC⊂SiO$_2$** with ultrasonication (Fig. 8). Both methods showed live bacteria with negligible change in biofilm viability in the control (93.5 ± 4.1%, 4.3 ± 1.0 × 10^7 CFU per mL) and when treated with ultrasound only (92.0 ± 5.3%, 5.6 ± 1.6 × 10^7 CFU per mL). **SiO$_2$** (10 mg mL^{-1}) also exhibited the same behaviour and no change in viability was observed (96.2 ± 2.7%, 4.7 ± 1.2 × 10^7 CFU per mL). Treatment of *S. sanguinis* biofilms with CPC (14 μg mL^{-1}) showed a reduction in live bacteria to 60.4 ± 10.8% which decreases to 45.7 ± 18.1% with ultrasound ($p > 0.1$), in both cases, there is a less than 100-fold ($<2 - \log 10$) reduction of CFU. A concentration of 14 μg mL^{-1} was chosen as it represents the average CPC release from **m-CPC⊂SiO$_2$** measured by UV-Vis spectroscopy under biofilm treatment conditions (Fig. S13†). After treatment with CPC (14 μg mL^{-1}) the analysis of bacterial cell viability across the biofilm showed highly variable viability, which overall is not significantly different ($p > 0.1$) when ultrasound is applied. There is high variability in percentage viability shown after CPC treatment (Fig. S14†). It is known that the diffusion of CPC in oral biofilms is slowed by an increase in extracellular polymeric substances density.[70] In addition, the CPC micelle structure could experience steric exclusion from a biofilm matrix causing bio accumulation in the antimicrobial agent in certain regions.[71] Furthermore, more killing is observed at further distances in biofilm after application of ultrasound. CPC mouth rinse formulations have been shown to only effect layers closer to the surface for biofilms grown for 48 h,[72] but introducing adjunct mechanical stress factors such as using a Phillips sonicate AirFloss to generate high-velocity microsprays found bacterial killing depth increased from 20% to 80% using a 0.085% CPC solution.[73] The combination of CPC with silica particles in **m-CPC⊂SiO$_2$** remarkably improved the performance of CPC due to enhanced penetration in biofilms and the increased localised dose of CPC which results in more bacteria killing in the biofilm. As expected from the disk diffusion assays, **m-CPC⊂SiO$_2$** (10 mg mL^{-1}) without ultrasound showed high biofilm viability (91.2 ± 5.0%, 1.1 ± 0.1 × 10^6 CFU per mL). However, the combination of ultrasound and drug release from **m-CPC⊂SiO$_2$** (10 mg mL^{-1}) reduced bacterial viability to

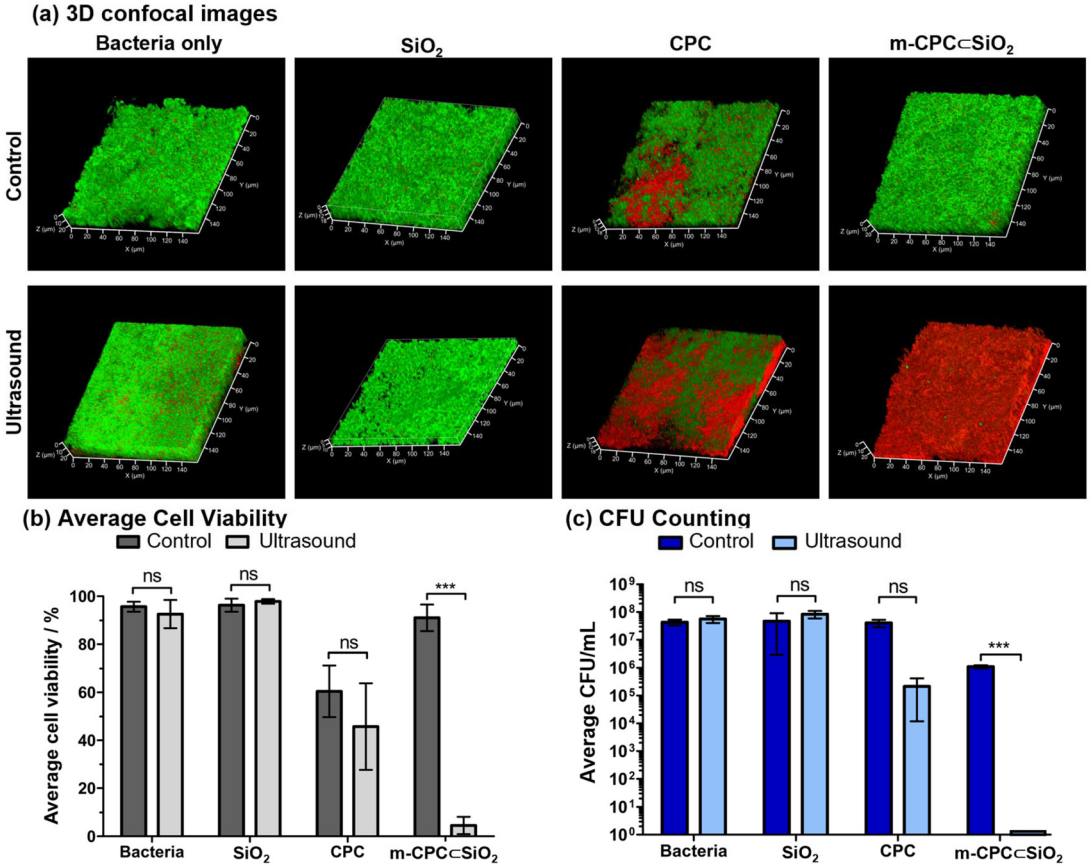

Fig. 8 3D confocal fluorescence microscopy of *S. sanguinis* biofilms showing the effect of particles before and after ultrasound and quantification of biofilm viability. (a) Images of biofilms following treatment with: plain SiO_2 (10 mg mL^{-1}), CPC (14 μg mL^{-1}) and **m-CPC⊂SiO$_2$** (10 mg mL^{-1}), before and post ultrasound (P10, 10 s) followed by 30 min incubation. Increments (*X*,*Y* axes) = 20 μm. Quantification of biofilm viability: (b) by live/dead staining, processing *z*-stack 3D images with ImageJ viability checker and (c) CFU counting, mean and standard deviation of analysis of biofilms tested for statistical significance using non-parametric Mann Whitney *U* test ($p < 0.05$). Five random areas of each biofilm were analysed, and experiments repeated in triplicate.

7.6 ± 4.5%. The cell viability was reduced by 1 000 000-fold (>6 log 10 reduction) compared to the control **m-CPC⊂SiO$_2$** without cavitation, when quantified using the CFU method ($p < 0.0001$). These results illustrate successful ultrasound triggered drug release of CPC encapsulated in silica particles for treatment and killing of single species mature biofilms, with a synergistic effect of ultrasound and **m-CPC⊂SiO$_2$**. Results from an MTT assay on oral keratinocytes (H400) demonstrated that the cytotoxicity of **m-CPC⊂SiO$_2$** is due to the encapsulated CPC drug. The unloaded particles, **SiO$_2$** showed 100% cell viability in the concentration up to 50 mg mL^{-1}. CPC alone shows a significant difference in cytotoxicity compared to the untreated control from 8–256 μg mL^{-1}. While **m-CPC⊂SiO$_2$** has no difference in cytotoxicity compared to the untreated control up to 2.5 mg mL^{-1} (Fig. S15†). The loading of CPC in **m-CPC⊂SiO$_2$** corresponds to a total of 192 μg_{CPC} (in 2.5 mg mL^{-1} nanoparticles), which highlights that encapsulation of CPC in the nanoparticles, reduces the cytotoxicity of CPC at high drug concentrations. The quantity of drug released from 10 mg mL^{-1} particles (14 μg mL^{-1}) equates to a greater than 75% cell viability. These MTT assays should be considered as a reference as despite possessing a level of toxicity towards cells, CPC is widely used as an antiseptic in the medical and dental fields.[22,45] It is important to note that the content of CPC amounts to 1 mg ml^{-1} in commercial products and approximately consumer safety and the CPC content in **m-CPC⊂SiO$_2$** is estimated to be 0.77 mg in 10 mg ml^{-1} which is below the maximum recommended concentration.[74]

Summary and outlook

This work presents low frequency ultrasound as an efficient stimulus for antimicrobial drug release from particles with an encapsulated agent. The delivery system **m-CPC⊂SiO$_2$** is a novel approach for one-pot synthesis with efficient encapsulation of CPC for potential dental applications. The structural changes of drug-loaded silica nanoparticles upon application of low frequency ultrasound are presented for the first time by high resolution electron microscopy, supporting the presence and release of the CPC agent. The **m-CPC⊂SiO$_2$** drug delivery system shows remarkable static stability and no activity in disk

diffusion assays towards *S. sanguinis*. On exposure to ultrasound produced from a hand-held dental scaler, **m-CPC⊂SiO$_2$** demonstrates triggered release enabling site specific treatment with CPC which is distinct from "burst" release of drug absorbed in MCM-41 particles Mono-species biofilms of *S. sanguinis* treated with **m-CPC⊂SiO$_2$** confirmed a significant synergistic antibiofilm effect against bacteria only in the presence of both ultrasound and **m-CPC⊂SiO$_2$**, improving the antibiofilm activity of CPC alone. This work suggests the potential application of **m-CPC⊂SiO$_2$** triggered by ultrasound as a novel drug delivery system to combat biofilms and to overcome challenges in delivery of drug molecules into intricate, anatomical structures inside the human tooth providing antibacterial treatment. The same approach could be applicable to a range of drugs in a range of clinical settings beyond dentistry.

Author contributions

Investigation and methodology: M. Manhota, M. L. Odyniec, G. Ball, F. Wang, R. Firdaus. Writing of original draft: M. Manhota, M. L. Odyniec. Further image analysis and writing: D. J. Bell. Project supervision: Y.-L. Chui, R. L. Sammons, S. A. Kuehne, A. D. Walmsley, Z. Pikramenou. Writing – review & editing: D. Bell, M. L. Odyniec, M. Manhota, G. Ball, S. A. Kuehne, A. D. Walmsley, Z. Pikramenou. Conceptualization: M. Manhota, S. A. Kuehne, A. D. Walmsley, Z. Pikramenou.

Conflicts of interest

There are no conflicts of interest to declare.

Data availability

The data supporting this article have been included as part of the ESI.†

Acknowledgements

The authors wish to acknowledge funding from: Engineering and Physical Sciences Research Council EP/L016346/1 (MM) and EP/V028553/1 (MLO, GB, ADW, SAK, ZP) as well as University of Birmingham (MM, GB).

References

1 N. B. Pitts, D. T. Zero, P. D. Marsh, K. Ekstrand, J. A. Weintraub, F. Ramos-Gomez, J. Tagami, S. Twetman, G. Tsakos and A. Ismail, *Nat. Rev. Dis. Primers*, 2017, **3**, 1–16.
2 J. N. Vergnes and M. Mazevet, *Lancet*, 2020, **395**, 186–186.
3 A. J. Righolt, M. Jevdjevic, W. Marcenes and S. Listl, *J. Dent. Res.*, 2018, **97**, 501–507.
4 H. C. Flemming and J. Wingender, *Nat. Rev. Microbiol.*, 2010, **8**, 623–633.
5 R. M. Donlan and J. W. Costerton, *Clin. Microbiol. Rev.*, 2002, **15**, 167–193.
6 C. A. Fux, J. W. Costerton, P. S. Stewart and P. Stoodley, *Trends Microbiol.*, 2005, **13**, 34–40.
7 M. K. Yadav, J.-J. Song, B. P. Singh and J. E. Vidal, in *New and Future Developments in Microbial Biotechnology and Bioengineering: Microbial Biofilms*, ed. M. K. Yadav and B. P. Singh, Elsevier, 2020, ch. 1, pp. 1–13.
8 D. Kim, J. P. Barraza, R. A. Arthur, A. Hara, K. Lewis, Y. Liu, E. L. Scisci, E. Hajishengallis, M. Whiteley and H. Koo, *Proc. Natl. Acad. Sci. U. S. A.*, 2020, **117**, 12375–12386.
9 N. Vyas, M. Grewal, S. A. Kuehne, R. L. Sammons and A. D. Walmsley, *Dent. Mater.*, 2020, **36**, 733–743.
10 C. M. L. Bollen, P. Lambrechts and M. Quirynen, *Dent. Mater.*, 1997, **13**, 258–269.
11 A. D. Walmsley, S. C. Lea, B. Felver, D. C. King and G. J. Price, *Clin. Oral Investig.*, 2013, **17**, 1227–1234.
12 C. E. Brennen, *Cavitation and Bubble Dynamics*, Cambridge University Press, New York, 2014.
13 N. Takahashi and B. Nyvad, *J. Dent. Res.*, 2011, **90**, 294–303.
14 W. H. Bowen, R. A. Burne, H. Wu and H. Koo, *Trends Microbiol.*, 2018, **26**, 229–242.
15 S. Oda, H. Nitta, T. Setoguchi, Y. Izumi and I. Ishikawa, *Periodontol. 2000*, 2004, **36**, 45–58.
16 G. Greenstein, *J. Am. Dent. Assoc.*, 2000, **131**, 1580–1592.
17 J. R. Kina, J. Kina, E. F. U. Kina, M. Kina and A. M. P. Soubhia, *J. Appl. Oral Sci.*, 2008, **16**, 205–208.
18 V. Mamaeva, C. Sahlgren and M. Linden, *Adv. Drug Delivery Rev.*, 2013, **65**, 689–702.
19 C. A. Stewart, Y. Finer and B. D. Hatton, *Sci. Rep.*, 2018, **8**, 895.
20 C. J. Seneviratne, K. C. F. Leung, C. H. Wong, S. F. Lee, X. Li, P. C. Leung, C. B. S. Lau, E. Wat and L. J. Jin, *PLoS One*, 2014, **9**, e103234.
21 O. V. Dement'eva and V. M. Rudoy, *RSC Adv.*, 2016, **6**, 36207–36210.
22 A. Brezhnev, F. K. Tang, C. S. Kwan, M. S. Basabrain, J. K. H. Tsoi, J. P. Matinlinna, P. Neelakantan and K. C. F. Leung, *ACS Appl. Bio Mater.*, 2023, **6**, 1221–1230.
23 H. J. Kim, H. Matsuda, H. S. Zhou and I. Honma, *Adv. Mater.*, 2006, **18**, 3083–3088.
24 X. A. Li, T. Tang, Y. Zhou, Y. F. Zhang and Y. H. Sun, *Microporous Mesoporous Mater.*, 2014, **184**, 83–89.
25 A. Bernardos, E. Aznar, M. D. Marcos, R. Martinez-Manez, F. Sancenon, J. Soto, J. M. Barat and P. Amoros, *Angew. Chem., Int. Ed.*, 2009, **48**, 5884–5887.
26 Q. L. Li, S. H. Xu, H. Zhou, X. Wang, B. A. Dong, H. Gao, J. Tang and Y. W. Yang, *ACS Appl. Mater. Interfaces*, 2015, **7**, 28656–28664.
27 L. Yuan, Q. Q. Tang, D. Yang, J. Z. Zhang, F. Y. Zhang and J. H. Hu, *J. Phys. Chem. C*, 2011, **115**, 9926–9932.
28 H. Kim, S. Kim, C. Park, H. Lee, H. J. Park and C. Kim, *Adv. Mater.*, 2010, **22**, 4280–4283.
29 L. Maggini, I. Cabrera, A. Ruiz-Carretero, E. A. Prasetyanto, E. Robinet and L. De Cola, *Nanoscale*, 2016, **8**, 7240–7247.

30 M. Frasconi, Z. C. Liu, J. Y. Lei, Y. L. Wu, E. Strekalova, D. Malin, M. W. Ambrogio, X. Q. Chen, Y. Y. Botros, V. L. Cryns, J. P. Sauvage and J. F. Stoddart, *J. Am. Chem. Soc.*, 2013, **135**, 11603–11613.
31 E. Aznar, L. Mondragon, J. V. Ros-Lis, F. Sancenon, M. D. Marcos, R. Martinez-Manez, J. Soto, E. Perez-Paya and P. Amoros, *Angew. Chem., Int. Ed.*, 2011, **50**, 11172–11175.
32 P. J. Chen, S. H. Hu, C. S. Hsiao, Y. Y. Chen, D. M. Liu and S. Y. Chen, *J. Mater. Chem.*, 2011, **21**, 2535–2543.
33 C. R. Thomas, D. P. Ferris, J. H. Lee, E. Choi, M. H. Cho, E. S. Kim, J. F. Stoddart, J. S. Shin, J. Cheon and J. I. Zink, *J. Am. Chem. Soc.*, 2010, **132**, 10623–10625.
34 J. L. Paris, P. de la Torre, M. V. Cabanas, M. Manzano, A. I. Flores and M. Vallet-Regi, *Acta Biomater.*, 2019, **83**, 372–378.
35 T. S. Anirudhan and A. S. Nair, *J. Mater. Chem. B*, 2018, **6**, 428–439.
36 J. L. Paris, M. V. Cabanas, M. Manzano and M. Vallet-Regi, *ACS Nano*, 2015, **9**, 11023–11033.
37 J. J. Wang, Y. J. Jiao and Y. R. Shao, *Materials*, 2018, **11**, 2041.
38 X. C. Li, Z. H. Wang and H. S. Xia, *Front. Chem.*, 2019, **7**, 59.
39 D. J. Lewis, V. Dore, N. J. Rogers, T. K. Mole, G. B. Nash, P. Angeli and Z. Pikramenou, *Langmuir*, 2013, **29**, 14701–14708.
40 D. J. Lewis, V. Dore, M. J. Goodwin, A. C. Savage, G. B. Nash, P. Angeli and Z. Pikramenou, *Meas. Sci. Technol.*, 2012, **23**, 084004.
41 A. R. Muguruza, A. di Maio, N. J. Hodges, J. M. A. Blair and Z. Pikramenou, *Nanoscale Adv.*, 2023, **5**, 2453–2461.
42 A. R. Muguruza, M. L. Odyniec, M. Manhota, Z. Habib, K. Rurack, J. M. A. Blair, S. A. Kuehne, A. D. Walmsley and Z. Pikramenou, *Microporous Mesoporous Mater.*, 2024, **363**, 112841.
43 S. Claire, A. D. Walmsley, S. Glinton, H. Floyd, R. Sammons and Z. Pikramenou, *J. Dent.*, 2015, **43**, 1242–1248.
44 N. Vyas, R. L. Sammons, Z. Pikramenou, W. M. Palin, H. Dehghani and A. D. Walmsley, *J. Dent.*, 2017, **56**, 112–120.
45 X. J. Mao, D. L. Auer, W. Buchalla, K. A. Hiller, T. Maisch, E. Hellwig, A. Al-Ahmad and F. Cieplik, *Antimicrob. Agents Chemother.*, 2020, **64**, DOI: 10.1128/aac.00576-20.
46 I. Molinero, M. L. Sierra, M. Valiente and E. Rodenas, *J. Chem. Soc., Faraday Trans.*, 1996, **92**, 59–63.
47 L. Zhu and J. Kreth, *Oxid. Med. Cell. Longevity*, 2012, **2012**, 717843.
48 S. S. Socransky, A. D. Haffajee, C. Smith and S. Dibart, *J. Clin. Periodontol.*, 1991, **18**, 766–775.
49 S. Renvert, T. Pettersson, O. Ohlsson and G. R. Persson, *J. Periodontol.*, 2006, **77**, 1110–1119.
50 L. Y. Zheng, A. Itzek, Z. Y. Chen and J. Kreth, *Int. J. Oral Sci.*, 2011, **3**, 82–89.
51 X. Guo, S. Liu, X. Zhou, H. Hu, K. Zhang, X. Du, X. Peng, B. Ren, L. Cheng and M. Li, *Sci. Rep.*, 2019, **9**, 6689.
52 C. T. Kresge, M. E. Leonowicz, W. J. Roth, J. C. Vartuli and J. S. Beck, *Nature*, 1992, **359**, 710–712.
53 E. Stride and C. Coussios, *Nat. Rev. Phys.*, 2019, **1**, 495–509.
54 N. Vyas, H. Dehghani, R. L. Sammons, Q. X. Wang, D. M. Leppinen and A. D. Walmsley, *Ultrasonics*, 2017, **81**, 66–72.
55 W. Lauterborn, T. Kurz, R. Geisler, D. Schanz and O. Lindau, *Ultrason. Sonochem.*, 2007, **14**, 484–491.
56 A. Prosperetti, *J. Acoust. Soc. Am.*, 1977, **61**, 17–27.
57 M. H. Entezari and P. Kruus, *Ultrason. Sonochem.*, 1994, **1**, S75–S79.
58 T. T. Nguyen, Y. Asakura, S. Koda and K. Yasuda, *Ultrason. Sonochem.*, 2017, **39**, 301–306.
59 G. A. Husseini, M. A. D. de la Rosa, E. S. Richardson, D. A. Christensen and W. G. Pitt, *J. Controlled Release*, 2005, **107**, 253–261.
60 A. Elamir, S. Ajith, N. Al Sawaftah, W. Abuwatfa, D. Mukhopadhyay, V. Paul, M. H. Al-Sayah, N. Awad and G. A. Husseini, *Sci. Rep.*, 2021, **11**, 7545.
61 A. Schroeder, Y. Avnir, S. Weisman, Y. Najajreh, A. Gabizon, Y. Talmon, J. Kost and Y. Barenholz, *Langmuir*, 2007, **23**, 4019–4025.
62 F. C. Lin, Y. J. Xie, T. Deng and J. I. Zink, *J. Am. Chem. Soc.*, 2021, **143**, 6025–6036.
63 R. Pazo-Llorente, C. Bravo-Diaz and E. Gonzalez-Romero, *Langmuir*, 2003, **19**, 9142–9146.
64 F. A. Pitten and A. Kramer, *Arzneimittelforschung*, 2001, **51**, 588–595.
65 N. Vyas, K. Manmi, Q. X. Wang, A. J. Jadhav, M. Barigou, R. L. Sammons, S. A. Kuehne and A. D. Walmsley, *Ultrasound Med. Biol.*, 2019, **45**, 1044–1055.
66 N. Vyas, E. Pecheva, H. Dehghani, R. L. Sammons, Q. X. Wang, D. M. Leppinen and A. D. Walmsley, *PLoS One*, 2016, **11**, e0149804.
67 S. E. Mountcastle, N. Vyas, V. M. Villapun, S. C. Cox, S. Jabbari, R. L. Sammons, R. M. Shelton, A. D. Walmsley and S. A. Kuehne, *NPJ Biofilms Microbiomes*, 2021, **7**, 44.
68 R. P. Howlin, S. Fabbri, D. G. Offin, N. Symonds, K. S. Kiang, R. J. Knee, D. C. Yoganantham, J. S. Webb, P. R. Birkin, T. G. Leighton and P. Stoodley, *J. Dent. Res.*, 2015, **94**, 1303–1309.
69 N. Vyas, R. L. Sammons, O. Addison, H. Dehghani and A. D. Walmsley, *Sci. Rep.*, 2016, **6**, 32694.
70 C. Sandt, J. Barbeau, M. A. Gagnon and M. Lafleur, *J. Antimicrob. Chemother.*, 2007, **60**, 1281–1287.
71 L. Marcotte, H. Therien-Aubin, C. Sandt, J. Barbeau and M. Lafleur, *Biofouling*, 2004, **20**, 189–201.
72 J. B. Xiang, H. M. Li, B. Q. Pan, J. L. Chang, Y. Y. He, T. He, R. Strand, Y. M. Shi and W. L. Dong, *Am. J. Dent.*, 2018, **31**, 53–60.
73 S. Fabbri, D. A. Johnston, A. Rmaile, B. Gottenbos, M. De Jager, M. Aspiras, E. M. Starke, M. T. Ward and P. Stoodley, *J. Dent. Res.*, 2016, **95**, 1494–1500.
74 Scientific Committee on Consumer Safety, *Revision of the opinion on Cetylpyridinium chloride - Submission II (P97)*, European Commission, 2015.